

The low-temperature dynamics of recovered ice XII as studied by differential scanning calorimetry: a comparison with ice V

Christoph G. Salzmann, Ingrid Kohl, Thomas Loerting, Erwin Mayer and Andreas Hallbrucker*

Institute of General, Inorganic and Theoretical Chemistry, University of Innsbruck, A-6020, Innsbruck, Austria. E-mail: andreas.hallbrucker@uibk.ac.at

Received 21st May 2003, Accepted 18th June 2003

First published as an Advance Article on the web 4th July 2003

Samples of ice XII made on isobaric heating of high-density amorphous ice (HDA) were recovered at 77 K and characterized by X-ray diffraction. Studies by differential scanning calorimetry (DSC) revealed, in addition to the intense exotherm from the ice XII \rightarrow cubic ice transition, on heating at 30 K min^{-1} a reversible endothermic step with an onset temperature (T_{onset}) of $130 \pm 1 \text{ K}$, an increase in heat capacity (ΔC_p) of $1.9 \pm 0.2 \text{ J K}^{-1} \text{ mol}^{-1}$, and a width of $10 \pm 1 \text{ K}$. The effects of the annealing temperature (T_{anneal}) for a fixed annealing time (t_{anneal}), and of t_{anneal} for a fixed T_{anneal} on the enthalpy and entropy relaxations and recovery have been ascertained, and these are phenomenologically similar to those of a glass. Ice XII samples made at 77 K on pressurizing of hexagonal ice *via* HDA show an additional thermal effect, namely an irreversible exotherm centered at 133 (125) K on heating at 30 (10) K min^{-1} , which is attributed to stress/strain release. For comparison, recovered ice V samples were studied by DSC in the same manner. These also show, in addition to the exotherm from the ice V \rightarrow cubic ice transition, on first heating at 30 K min^{-1} a reversible endothermic step with T_{onset} of $130 \pm 1 \text{ K}$, ΔC_p of $1.7 \pm 0.2 \text{ J K}^{-1} \text{ mol}^{-1}$, and width of $20 \pm 1 \text{ K}$, and annealing effects similar to those of ice XII. For ice V the existence of a temperature-dependent equilibrium between proton order and disorder, with proton order increasing with decreasing temperature, had been ascertained by Lobban *et al.* (*J. Chem. Phys.*, 2000, **112**, 7169). We thus interpret the endothermic step in unannealed ice V to kinetic unfreezing of proton order–disorder, the equilibrium line being attained by proton order \rightarrow disorder transition, and the effects of annealing to enthalpy and entropy loss during annealing by approaching the proton order–disorder equilibrium, and on their subsequent recovery on reheating, in line with Handa *et al.* (*J. Phys.* 1987, **48**, C1-435). The endothermic DSC features of ice XII are interpreted in the same manner, by relaxation of the frozen-in proton order–disorder towards equilibrium *via* proton order \rightarrow disorder transition. For ice XII (ice V) the maximal value of recovered configurational entropy corresponds to $0.17 \text{ J K}^{-1} \text{ mol}^{-1}$ ($0.22 \text{ J K}^{-1} \text{ mol}^{-1}$) after annealing at 115 K for 120 min (111 K for 90 min) which is 5.0% (6.5%) of the maximal value of $3.37 \text{ J K}^{-1} \text{ mol}^{-1}$ for complete proton order \rightarrow disorder transition. We further report the DSC features of low-density amorphous ice recorded on heating at 30 K min^{-1} , with T_{onset} of an endothermic step at $134 \pm 2 \text{ K}$ and ΔC_p of $0.7 \pm 0.1 \text{ J K}^{-1} \text{ mol}^{-1}$, and we show the similarities of this endothermic feature to those of ice XII.

Introduction

The polymorphic forms of ice illustrate the structural variety possible for the hydrogen-bonded polymers of four-coordinated water, and studies of the crystalline phases of ice, in which the water molecules form tetrahedral networks by hydrogen bonding, and of proton order–disorder phenomena are important for further understanding of the hydrogen bond. The recent discovery of a new phase of ice, ice XII, was reported in 1998 by Lobban *et al.*¹ who prepared and characterized it by slow crystallization from the liquid phase at 260 K at a pressure of 0.55 GPa, which is within the stability region of ice V.² Ice XII “contains only seven- and eight-membered rings and is the first example of a 4-connected net of this type”.³ In the same year Chou *et al.*⁴ reported a new “High-Pressure Phase of H_2O Ice” in the ice VI domain, at 0.7 to 1.2 GPa and melting temperatures of between 3 to 26 °C (Table I in ref. 4). They speculated on the relation of their new phase to ice XII reported by Lobban *et al.*¹ but, because of the lack of data, could not confirm it or rule it out (note 24 in ref. 4). Subsequently to formation of ice XII from the liquid phase,¹ Koza *et al.*⁵ reported formation of ice XII in a completely different region of water’s phase diagram, namely as an incidental product in the preparation of high-density

amorphous ice (HDA)^{6–9} at 77 K on compression of hexagonal ice (ice Ih) up to 1.8 GPa. Kohl *et al.*¹⁰ then showed that in this route ice XII forms on compression of ice Ih only *via* HDA, and not directly from ice Ih, and that its formation requires a sudden pronounced pressure drop at pressures $\gtrsim 1.1 \text{ GPa}$. They further proposed that “shock-waves generated by the pressure drops cause transient local heating up to the temperature range of the ice V domain, and that this induces nucleation and crystal growth of ice XII.” This explains why in this route the relative amounts of HDA and ice XII were scattered more or less randomly.⁵ An important improvement is that pure ice XII can now be prepared in a reproducible manner in gram-quantities, without contamination by HDA and low-density amorphous ice (LDA), by isobaric heating of HDA kept at a pressure of 0.8 GPa up to 195 K at a rate of $\gtrsim 15 \text{ K min}^{-1}$.^{11–15} Raman spectroscopic studies of ice XII (ref. 12) suggest that the new “High-Pressure Phase of H_2O Ice” reported by Chou *et al.*⁴ in the ice VI domain is in fact ice XII. Moreover, Raman spectra of ice XII (ref. 12) indicate proton-disorder which is consistent with the positional disorder of hydrogen atoms from analysis of diffraction data.¹

In our first study of the thermal properties of ice XII by differential scanning calorimetry (DSC)¹⁶ we concluded that ice XII is metastable with respect to ice V. Our subsequent DSC

studies of pure ice XII (made on isobaric heating of HDA under pressure, that is without contamination by HDA/LDA, *cf.* refs. 11–15) showed that the thermal features of ice XII at low-temperatures, below the ice XII \rightarrow cubic ice (ice Ic) phase transition, are obscured in the presence of an HDA contamination by those of HDA/LDA.¹⁷ These low-temperature DSC features of pure recovered ice XII become clearly observable in the absence of HDA/LDA, and they are reported here and compared with those of ice V. The remarkable similarity between the DSC scans of ice XII and ice V observed in this study at low-temperatures is attributed to partial proton ordering which is in line with the calorimetric study of ice V by Handa *et al.*¹⁸

We further compare DSC scans of HDA and LDA with those of ice XII because their thermal features are in several respects very similar and thus were mistaken in earlier studies.^{19–23}

Experimental

Ice XII was prepared on isobaric heating of HDA without pressure drops.^{11–15} This gives pure ice XII, without contamination by HDA and/or LDA, and it is, therefore, described briefly as follows: 0.300 cm³ of deionized H₂O were pipetted into a precooled piston-cylinder apparatus with an 8 mm diameter piston, and HDA was made by compression of ice Ih at 77 K with indium linings up to 1.6 GPa. This HDA was subsequently heated at a constant pressure of 0.81 GPa up to 195 K at a rate of ≈ 16 K min⁻¹ where its phase transition generated pure ice XII.^{11–15} Samples were cooled in the piston-cylinder apparatus under pressure to 77 K at a rate of ≈ 50 K min⁻¹, recovered under liquid N₂ at 1 bar, and then characterized by X-ray diffraction. The samples were compressed with a computerized “universal testing machine” (Zwick, Model BZ100/TL3S) at a rate of 7000 N min⁻¹. Its positional reproducibility is ± 5 μ m, and the spatial resolution of the drive is 0.01 μ m. Pressure displacement curves were recorded with the TestXpert V 7.1 Software of Zwick. Temperature was measured with a thermocouple firmly attached to the outside of the piston cylinder apparatus, and the accuracy is estimated as ± 2 K by following the glass-liquid transition of glycerol at ambient pressure for calibration.

Alternatively, ice XII samples containing varying amounts of HDA/LDA were prepared by compression of ice Ih at 77 K up to ≥ 1.1 GPa without indium linings.^{5,10,17,24} Under these conditions apparent pressure drops can cause transient local heating by shock-waves, up to the temperature range of the ice XII metastability domain.¹¹ Recovered ice XII prepared in this manner was characterized by X-ray diffraction as described above.

Ice V was prepared by compression of ice Ih between 238–250 K up to 0.64 GPa, and conversion of ice Ih to ice V was followed by the pressure *versus* displacement curve. The sample was subsequently cooled to 77 K with liquid N₂ at 0.64 GPa and, after release of pressure, it was recovered under liquid N₂ at 1 bar and characterized by its X-ray diffractogram.¹⁷

For preparation of LDA, first HDA was made by compression of ice Ih at 77 K up to 1.2 GPa, using indium linings in order to avoid pressure drops. Thereafter pressure was reduced to 0.025 GPa and sample and cell were heated isobarically up to 137 K. Conversion of HDA to LDA was followed by the temperature *versus* displacement curve. The sample was subsequently cooled to 77 K with liquid N₂, recovered under liquid N₂ at 1 bar and characterized by its X-ray diffractogram.¹⁷

A differential scanning calorimeter (Model DSC-4, Perkin-Elmer) with a self-written computer program was used. After heating each sample from 93 K up to 253 K (for Figs. 2 to 4) or to 273 K (for Figs. 6 to 9) and recording its DSC scan,

the sample was cooled to 93 K and a second heating scan of now ice Ih was recorded and subtracted as a baseline from the first scan. In our experience this procedure of generating a baseline is superior to that recommended by the manufacturer by using empty sample pans and applied in our first DSC study,²⁵ and these baseline-subtracted DSC scans are shown without further change of slope (except for Fig. 7). The DSC scans were recorded on heating at a rate of 10 or 30 K min⁻¹. Between 15.2 and 30.2 mg of sample were transferred under liquid N₂ into steel capsules with screwable lids. The mass of the sample was obtained *via* the melting endotherm of ice, by using the value of 6.012 kJ mol⁻¹ as heat of melting.²⁵ The DSC instrument was calibrated with cyclopentane. Temperature calibration of the instrument showed that thermal lag is negligible for heating at a rate of 10 K min⁻¹, and it is -1.6 K for heating at 30 K min⁻¹.

X-ray diffractograms were recorded on a diffractometer in θ - θ geometry (Siemens, model D 5000, Cu-K α), equipped with a low-temperature camera from Paar. The sample plate was in horizontal position during the whole measurement. Installation of a “Goebel mirror” allowed to record small amounts of sample without distortion of the Bragg peaks. Calculation of X-ray diffractograms was performed with the “Powder-Cell” Software (BAM, Bundesanstalt für Materialforschung, Berlin, Germany).

Results

Ice XII made on isobaric heating of HDA

Only when pure ice XII could be made, not contaminated by HDA/LDA as in our previous study¹⁶ or by other high-pressure ice,^{11,24} it became possible to investigate reliably its thermal features at low temperatures. Therefore we first show how pure ice XII is made and characterized, and then present in detail its DSC features. Fig. 1 shows the pressure-displacement (Δl) curve (a) obtained on compression of ice Ih at 77 K up to 1.6 GPa. This curve has the same shape as

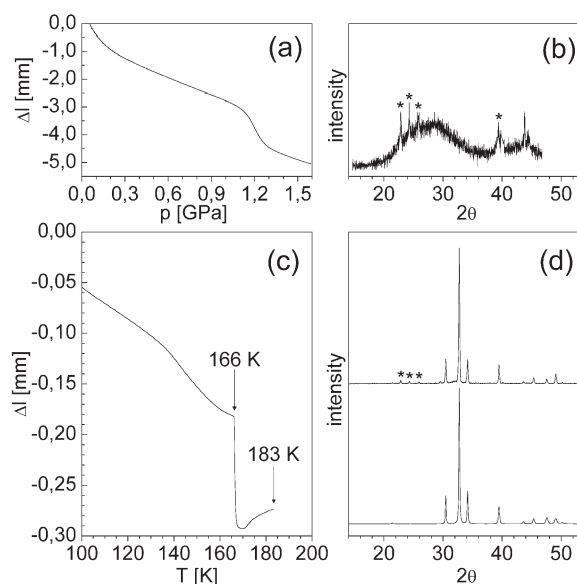


Fig. 1 Characterization of recovered ice XII by X-ray diffraction (Cu-K α). (a) is the displacement (Δl) *versus* pressure curve on compression of ice Ih at 77 K with indium lining; (b) the X-ray diffractogram of recovered HDA recorded at 90 K; (c) is the Δl *versus* temperature plot on isobaric heating of HDA at 0.81 GPa at a rate of *ca.* 16 K min⁻¹ up to 183 K (with indium lining); and (d) compares the X-ray diffractogram of recovered ice XII (top, recorded at *ca.* 90 K) with the simulated one (bottom). Three weak features marked with asterisks are from a minor amount of ice Ih.

pressure-displacement curves reported *e. g.* by Mishima *et al.*,^{6,7} and as that shown in Fig. 1a of ref. 10. The pronounced decrease in volume on compression above *ca.* 1.1 GPa is due to the phase transition of ice Ih to HDA. The transformation begins at slightly higher pressure than reported before^{6-9,26-29} which is attributed to friction in the piston-cylinder apparatus. The pressures given in the following are nominal pressures, and the pressures at the sample are expected to be slightly lower. These pressure-displacement curves without pressure drops are characteristic for formation of HDA without ice XII.¹⁰ HDA recovered after compression under liquid N₂ at 1 bar was characterized by X-ray diffraction. Its diffractogram (curve b) is that reported in the literature,⁶⁻⁹ with the maximum of the intense broad peak at 3.0 Å. Bragg peaks from a small amount of ice Ih are marked by asterisks. This ice Ih comes from condensation of water vapor during transfer of the sample into the precooled sample plate holder of the diffractometer, and not from untransformed ice Ih. This is consistent with our observation that Raman spectra of recovered H₂O HDA and H₂O ice XII containing 9 mol.% HOD did not show the decoupled O-D stretching band of ice Ih. HDA or ice XII samples containing ice Ih from its incomplete conversion would have shown this Raman band. In subsequent experiments HDA was made by compression of ice Ih at 77 K as described above and then heated isobarically without characterizing it by X-ray diffraction, and the absence of pressure drops in the Δl versus temperature plots is taken as indication for the absence of shock-wave heating.

Pure ice XII was obtained on isobaric heating of HDA at 0.81 GPa at a rate of *ca.* 16 K min⁻¹ (*cf.* Fig. 1c).¹¹⁻¹⁵ HDA first gradually densifies further on isobaric heating.^{8,9,11} Pronounced decrease in volume starts at 166 K (marked), indicating phase transition to a denser phase, and it ends at 169 K. After heating to 183 K (marked), the sample was cooled to liquid N₂ and recovered under liquid N₂ at 1 bar. Thereafter it was characterized by its X-ray diffractogram (*cf.* Fig. 1d, top) as pure ice XII by comparison with the simulated diffractogram (Fig. 1d, bottom) obtained from the structural data reported by Lobban *et al.*¹ A small amount of ice Ih is marked by asterisks (see above for its origin). For ice XII prepared in this manner contamination by HDA/LDA can be excluded because these transform into a crystalline phase under these *p-T* conditions.^{8,11} From inspection of the ice XII diffractogram at high gain and its signal-to-noise ratio we estimate that contamination by a crystalline phase other than ice Ih (marked) can be at most 1-2%.

Recovered ice XII samples prepared as described above were used for the DSC studies described in Figs. 2-4. Fig. 2 shows the DSC scan of a sample recorded on heating at 30 K min⁻¹ from 93 to 253 K (a). The intense exotherm from the ice XII → ice Ic transition has a peak minimum temperature of 162 K, and a weak broad feature at *ca.* 233 K is from the ice Ic → ice Ih transition. The total mass of the sample of 19.8 mg was determined from the area of the melting endotherm for a value of 6.012 kJ mol⁻¹ (not shown).²⁵ We found that the enthalpy of the ice XII → ice Ic transition could be determined more reliably from DSC scans recorded on slow heating at 10 K min⁻¹ because the absence of tailing allowed unambiguous integration of the peak area. From DSC scans of 15 samples (not shown), the ΔH value obtained in this manner is -1.20 ± 0.07 kJ mol⁻¹.¹⁷ This value compares well with our previous ΔH value of -1.27 ± 0.05 kJ mol⁻¹ for the ice XII → ice Ic transition obtained for ice XII made by compression of ice Ih and shockwave heating at 77 K.¹⁶ The latter ice XII contained varying amounts of HDA/LDA which had to be taken into account.

A further feature is a weak endothermic step below the intense exotherm which is recognizable in curve (a) even at low gain. This step becomes evident in (b) on 10-fold enlargement. The reversibility of this endothermic step is

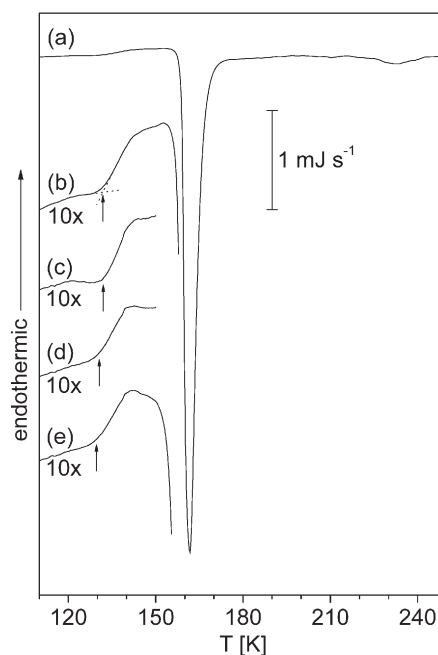


Fig. 2 DSC scans of recovered ice XII samples prepared on isobaric heating of HDA (outlined in Fig. 1): (a) is the scan of a 19.8 mg sample recorded on heating at 30 K min⁻¹ from 93 to 253 K, and (b) the low-temperature region 10-fold expanded. (c) is the scan of a new 13.2 mg sample obtained on first heating at 30 K min⁻¹ from 93 K to 150 K, (d) and (e) the scans of the same sample obtained on second heating to 150 K and on third heating to 253 K. The sample was cooled immediately at 30 K min⁻¹ to 93 K after recording scans (c) and (d) on heating to 150 K. The onset of the endothermic step (T_{onset}) was determined as indicated by the broken lines, determined as indicated by broken lines. The scans are normalized with respect to the samples' weights and shifted vertically for clarity. The ordinate bar is for (a) and 1 mg sample weight.

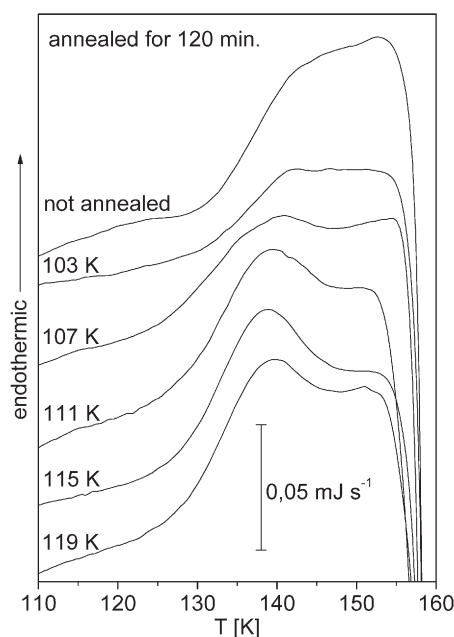


Fig. 3 The effect of annealing temperature (T_{anneal}) on the DSC scans of recovered ice XII prepared on isobaric heating of HDA: the top curve shows a scan of an unannealed sample recorded on heating at 30 K min⁻¹ from 93 to 253 K, and the scans below are for samples recorded, after annealing for 120 min at the given temperatures of between 103 to 119 K, on heating at 30 K min⁻¹, determined as indicated by broken lines. The scans are normalized with respect to the samples' weights and shifted vertically for clarity. The ordinate bar is for a 1 mg sample weight.

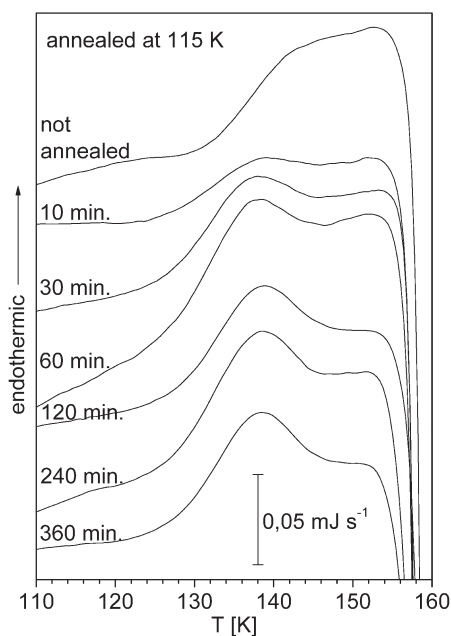


Fig. 4 The effect of annealing time (t_{anneal}) on the DSC scans of recovered ice XII prepared on isobaric heating of HDA: the top curve shows a scan of an unannealed sample recorded on heating at 30 K min^{-1} from 93 to 253 K, and the scans below are for samples recorded, after annealing at 115 K for t_{anneal} of between 10 to 360 min, on heating at 30 K min^{-1} , determined as indicated by broken lines. The scans are normalized with respect to the samples' weights and shifted vertically for clarity. The ordinate bar is for a 1 mg sample weight.

demonstrated by curves (c) to (e). Curve (c) is the DSC scan of a new sample heated at 30 K min^{-1} from 93 K up to 150 K. The sample was immediately cooled to 93 K at 30 K min^{-1} . Curve (d) is the scan recorded on second heating at 30 K min^{-1} up to 150 K. After immediate cooling of the sample to 93 K, curve (e) was recorded on third heating up to 253 K. The onset temperature of the endothermic step, T_{onset} , was determined by broken lines as indicated in (b), and it is marked by arrows. For curve (b) it is at 132 K and, after correction for the thermal lag of the instrument, T_{onset} is 130 K. A weak exothermic feature is observable on first heating near T_{onset} (curves (b) and (c)) which disappears on second heating (curves (d) and (e)). The increase in heat capacity, ΔC_p , of the endothermic step is $1.8 \text{ J K}^{-1} \text{ mol}^{-1}$, and its width is 9 degrees. For curves (c), (d) and (e) the corresponding values are for T_{onset} 130, 129 and 128 K (corrected for thermal lag), for ΔC_p 2.3, 1.6 and $1.8 \text{ J K}^{-1} \text{ mol}^{-1}$, and for width of 9, 9 and 10 K. The plateau region above 140 K in (b) and (c) disappears in (e) on third heating. We attribute this to nucleation and crystal growth of ice Ic which shifts the ice XII \rightarrow ice Ic exotherm to lower temperature. From the DSC scans of 4 further samples taken from 2 batches, T_{onset} is $130 \pm 1 \text{ K}$ (corrected), ΔC_p is $1.9 \pm 0.2 \text{ kJ mol}^{-1}$, and the width is 10 ± 1 degrees, and these values were obtained from ice XII samples on first heating.

The effect of annealing temperature, T_{anneal} , on the DSC scans of recovered ice XII is shown in Fig. 3. The top curve shows for comparison the scan on an unannealed sample recorded on heating at 30 K min^{-1} from 93 to 250 K. Samples were annealed by heating from 93 K to the temperature indicated in the figure at a rate 30 K min^{-1} , holding them for 120 min at this temperature, cooling to 93 K at 30 K min^{-1} , and finally by heating at a rate of 30 K min^{-1} and recording the DSC scan. These scans show that with increasing T_{anneal} an endothermic peak becomes more and more pronounced, and that this peak seems to have a maximum for $T_{\text{anneal}} = 115 \text{ K}$. These endothermic peak areas represent the recovered enthalpy, ΔH (reviewed in ref. 30).

The effect of annealing time, t_{anneal} , for $T_{\text{anneal}} = 115 \text{ K}$, on the DSC scans of recovered ice XII is shown in Fig. 4. The top curve shows again for comparison the scan of an unannealed sample recorded on heating at 30 K min^{-1} from 93 to 250 K. Samples were annealed by heating from 93 to 115 K at a rate of 30 K min^{-1} , holding them at 115 K for the time indicated in the figure, cooling to 93 K at 30 K min^{-1} , and finally by heating at a rate of 30 K min^{-1} and recording the DSC scan. These scans show that for short t_{anneal} (10 min) only a weak endothermic feature is observable, and that for long t_{anneal} a pronounced endothermic peak develops.

In Fig. 5 the recovered enthalpy, ΔH , is plotted versus T_{anneal} (data from Fig. 3) in curve (a), and versus t_{anneal} (data from Fig. 4) in curve (b). ΔH values were determined by subtracting first the scan of an unannealed sample from that of an annealed sample, and by integrating thereafter the resulting peak of the difference curve. Fig. 5(a) shows that ΔH has a maximum for T_{anneal} of 115 K, whereas in (b) ΔH approaches a constant value for t_{anneal} of ca. > 70 min. In a plot of ΔH versus $\ln(t_{\text{anneal}})$, leveling off also occurred at ca. 70 min and ΔH remained constant for longer t_{anneal} (not shown). This leveling off occurs when the enthalpy had relaxed fully toward the equilibrium line.³¹

In Fig. 5 further the recovered entropy, ΔS , is plotted in curve (c) versus T_{anneal} , and in curve (d) versus t_{anneal} . These ΔS values were calculated by integration from the ΔH values, with the temperature axis as $\ln(T)$. The dotted lines are inserted to aid the eye.

Ice XII made on compression of HDA at 77 K via pressure drop and shockwave heating

The DSC features of recovered ice XII made this way can easily be mistaken for those of HDA/LDA. Because of that we follow the recipe used in Fig. 1 of ref. 19 where the DSC features of pressure-amorphized ice Ih had been reported. Ice XII was made on compression of HDA at 77 K without indium lining,^{5,10} and Fig. 6 (top) shows the pressure versus displacement curve where a pronounced drop at 1.36 GPa caused transient local heating by a shockwave. The X-ray diffractogram of the recovered sample (middle) shows the pattern of ice XII,¹ indicating that HDA had transformed into ice XII. Several DSC scans of ice XII made in this manner are also shown in Fig. 6 (bottom). For differentiating between irreversible and reversible thermal effects, the same sample was heated several times to a selected temperature at 30 K min^{-1} , and cooled thereafter to 93 K at 30 K min^{-1} . Scans (a) to (d) were obtained with the same sample. Curve (a) was obtained on first heating from 93 to 123 K and shows the beginning of an exothermic feature. Reheating for a second time (curve (b)) to 143 K shows an exothermic peak with T_{min} at 132 K. Reheating for a third time (curve (c)) to 273 K shows that the exotherm had disappeared on heating to 143 K, and that in (c) an endothermic step becomes observable with an onset temperature, T_{onset} , of 132 K (marked by the arrow). Curve (d) is (c) depicted on a reduced (15-fold) scale, and it shows the exotherm from the ice XII \rightarrow ice Ic transition with T_{min} of 161 K.

A new sample from the same batch was used for scans (e) to (g), and these show in addition the effect of annealing at 127 K. Curve (e) was recorded on first heating from 93 to 143 K, after annealing at 127 K for 90 min, curve (f) was obtained on second heating from 93 to 273 K, and curve (g) is (f) shown on a reduced (15-fold) scale. The weak exotherm in curves (c) and (f) with T_{min} of 233 K is from the ice Ic \rightarrow ice Ih transition. The intense exotherm from the ice XII \rightarrow ice Ic transition shows in addition a weak exotherm at 172 K (d) or a shoulder (g). These features can be assigned to a minor amount of LDA transforming into ice Ic by comparison with our previous DSC study of ice XII containing varying amounts of HDA/LDA.¹⁶

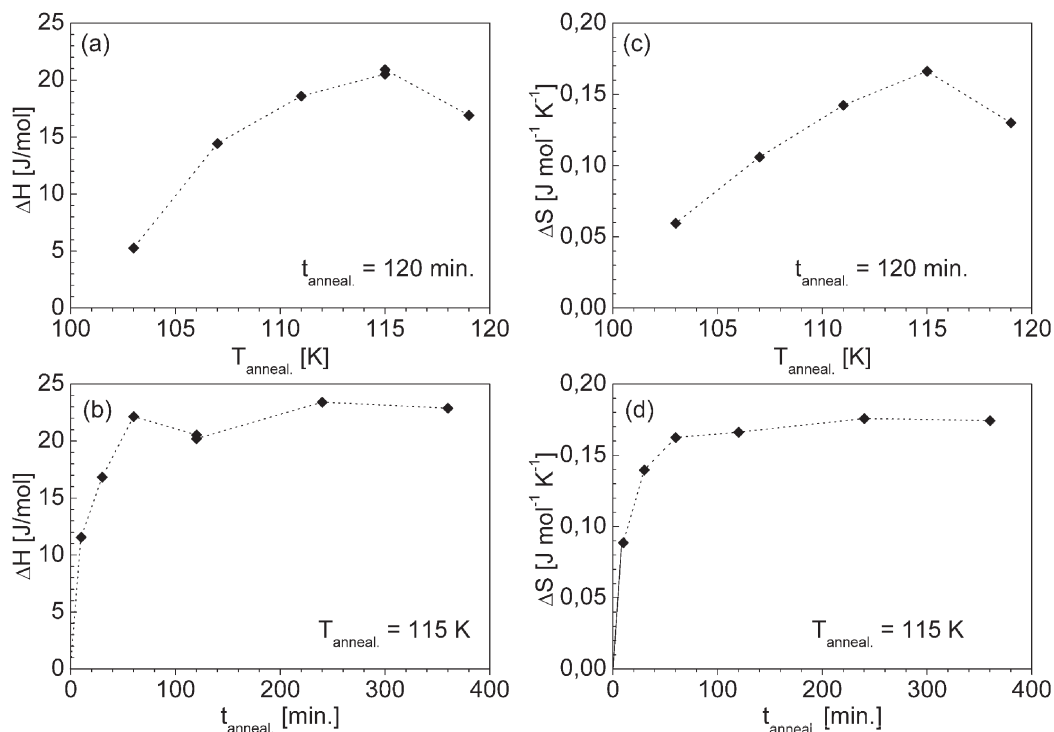


Fig. 5 (a) and (b) Plot of the recovered enthalpy, ΔH , versus T_{anneal} for constant t_{anneal} of 120 min (a, data from Fig. 3), or versus t_{anneal} for constant T_{anneal} of 115 K (b, data from Fig. 4). Endothermic peak areas were determined by first subtracting the scan of an unannealed sample from that of an annealed sample, and then by integrating the resulting peak in the difference curve. (c) and (d) Plot of the recovered entropy, ΔS , versus T_{anneal} for constant t_{anneal} of 120 min (c), or versus t_{anneal} for constant T_{anneal} of 115 K (d). The dotted lines are inserted to aid the eye.

Thus, apparently HDA had not transformed completely into ice XII on pressure drop and shockwave heating.

These DSC scans show that the exotherm with T_{min} of 132 K is an irreversible effect and disappears either on heating to 143 K ((b) versus (c)) or on annealing at 127 K (e). However, the endothermic step with T_{onset} of 129 K (marked by arrows) is a reversible effect (cf. curve (e) versus (f)). After correction for thermal lag of the instrument, T_{onset} is 128 K, ΔC_p is $1.7 \text{ J K}^{-1} \text{ mol}^{-1}$, and the width of the endothermic step is 10 K. Several more samples from different batches were studied by DSC, and the heat effect of the irreversible exotherm with T_{min} of $133 \pm 2 \text{ K}$ (T_{min} of $125 \pm 2 \text{ K}$ for heating at 10 K min^{-1}) was determined as $-42 \pm 14 \text{ J mol}^{-1}$.¹⁷

Comparison with LDA

Since the thermal features of LDA can easily be mistaken for those of ice XII, we next compare in Fig. 7 their DSC scans. LDA was made on isobaric heating of HDA at 0.025 GPa up to 137 K,^{6,7} and it was characterized by its X-ray diffractogram (cf. Fig. 7, top). Curve (a) shows the DSC scan of LDA recorded, after annealing at 129 K for 90 min, on heating from 93 K to 273 K, and curve (b) is (a) 15-fold enlarged. Curve (c) shows the DSC scan of ice XII recorded, after annealing at 127 K for 180 min, on heating from 93 K to 273 K, and curve (d) is (c) 15-fold enlarged. From this and other DSC scans of LDA the enthalpy of the LDA \rightarrow ice Ic exotherm was determined as $-1.37 \pm 0.06 \text{ kJ mol}^{-1}$,¹⁷ and thus is nearly the same as that reported by Handa *et al.* (cf. Table I in ref. 32). This exothermic heat effect is close to that determined for the ice XII \rightarrow ice Ic transition, with ΔH of $-1.20 \pm 0.07 \text{ kJ mol}^{-1}$, or $-1.27 \pm 0.05 \text{ kJ mol}^{-1}$ in ref. 16. A difference exists in that for heating at 30 K min^{-1} , T_{min} of the exotherm is at $171 \pm 1 \text{ K}$ for the LDA \rightarrow ice Ic transition whereas it is at $160 \pm 1 \text{ K}$ for ice XII \rightarrow ice Ic transition (corrected for thermal lag; on heating at 10 K min^{-1} T_{min} is at 155 and 166 K, cf. ref. 16). A weak exotherm from the transition of ice Ic to ice Ih is centered at ca. 246 K for (b) and at ca. 232 K for (d).

The enlarged curves (b) and (d) show both an endothermic feature below the intense exotherm. In curve (d) T_{onset} of the weak endothermic feature is at 129 K (marked by the arrow), and ΔC_p is $1.7 \text{ J K}^{-1} \text{ mol}^{-1}$. In curve (b) T_{onset} is at 135 K (marked by the arrow), and ΔC_p is $0.7 \text{ J K}^{-1} \text{ mol}^{-1}$. After correction for thermal lag, T_{onset} is at 128 K in (d) and 134 K in (b). The width of the endothermic step in (b) cannot be reliably determined because it seems to be cut off from the intense exotherm. From further DSC scans of 5 samples, the LDA values are reproducible to $\pm 2 \text{ K}$ and $\pm 0.1 \text{ J K}^{-1} \text{ mol}^{-1}$. This ΔC_p value is the same as that reported by Handa and Klug³³ on heating LDA at 10 K h^{-1} , after annealing at 129 or 130 K for 2 h. Thus, T_{onset} of the endothermic feature in ice XII is ca. 6 K lower than that of LDA, and the height of the step is more than twice that in LDA.

Comparison with recovered ice V

Handa *et al.*^{18,34} has reported endothermic features on heating and annealing of ice V which seemed similar to those observed here for ice XII. Comparison with their study is problematic because it was done with an adiabatic calorimeter on heating at a rate of 0.167 K min^{-1} instead of the 30 K min^{-1} used here. We therefore investigated the thermal features of recovered ice V by DSC in the same manner described above for ice XII. Ice V was made according to Bertie *et al.*³⁵ Recovered ice V was characterized by its X-ray diffractogram (cf. Fig. 8, top), and the d -spacings are those reported in ref. 35. Samples from the same batch were studied by DSC on heating and cooling at a rate of 30 K min^{-1} . Curve (a) in Fig. 8 shows the DSC scan of an ice V sample recorded on heating from 93 K to 273 K, and curve (b) is (a) 30-fold enlarged. The intense exotherm with T_{min} at 166 K is from the ice V \rightarrow ice Ic transition, and its enthalpy change, $\Delta H_{\text{ice V} \rightarrow \text{ice Ic}}$, is $-0.909 \text{ kJ mol}^{-1}$. From the DSC scans of 2 further ice V samples recorded on heating at 10 K min^{-1} ΔH values of -0.945 and $-0.925 \text{ kJ mol}^{-1}$ were obtained. Thus, $\Delta H_{\text{ice V} \rightarrow \text{ice Ic}}$ is

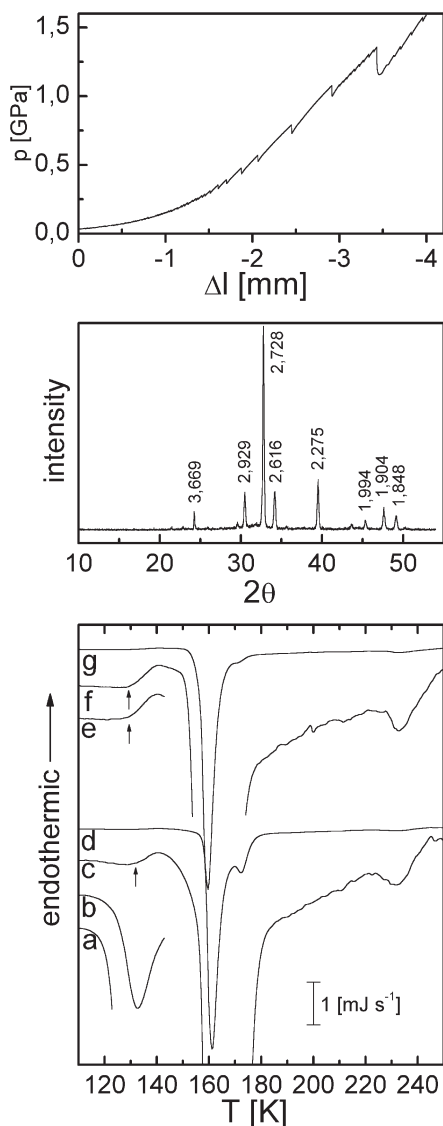


Fig. 6 Recovered ice XII made by compression of HDA at 77 K without indium lining *via* pressure drop and shockwave heating: the top curve shows the pressure *versus* displacement curve, with a pronounced pressure drop at 1.36 GPa by 0.20 GPa, the diffractogram (middle) characterizes the recovered material as ice XII. This ice XII was studied by DSC (bottom) on heating and cooling at 30 K min⁻¹ as follows: (a) was recorded on first heating to 123 K; (b) shows the heat released on second heating to 143 K, after cooling to 93 K; (c) shows an endothermic feature on third heating, after cooling to 93 K, of the same sample to 273 K; and (d) is curve (c) depicted on a reduced (15-fold) scale. (e) is the scan of a new sample recorded, after annealing at 127 K for 90 min, on first heating from 93 to 143 K; (f) the scan of the same sample recorded, after cooling to 93 K, on second heating to 273 K; and (g) is curve (f) shown on a reduced (15-fold) scale. The scans are normalized with respect to the samples' weights and shifted vertically for clarity. The ordinate bar is for (a) and 1 mg sample weight.

calculated as -0.926 ± 0.020 kJ mol⁻¹. This compares nicely with the value of -0.915 ± 0.004 kJ mol⁻¹ reported by Handa *et al.*^{18,34} Curves (b) and (d) further show weak exotherms centered at *ca.* 235 K from the ice Ic \rightarrow ice Ih transition.

Curve (b) shows in addition an endothermic step with T_{onset} at 132 K (marked by the arrow), ΔC_p of 1.6 J K⁻¹ mol⁻¹ and width of *ca.* 20 K. To test for reversibility of the endothermic step, the DSC scan of a new ice V sample recorded on first heating from 93 K to 150 K is shown as curve (c), and on second heating of the same sample to 273 K as curve (d). Both curves (c) and (d) are also shown 30-fold enlarged. T_{onset} (marked by arrows), ΔC_p and width are 132 K, 1.6 J K⁻¹

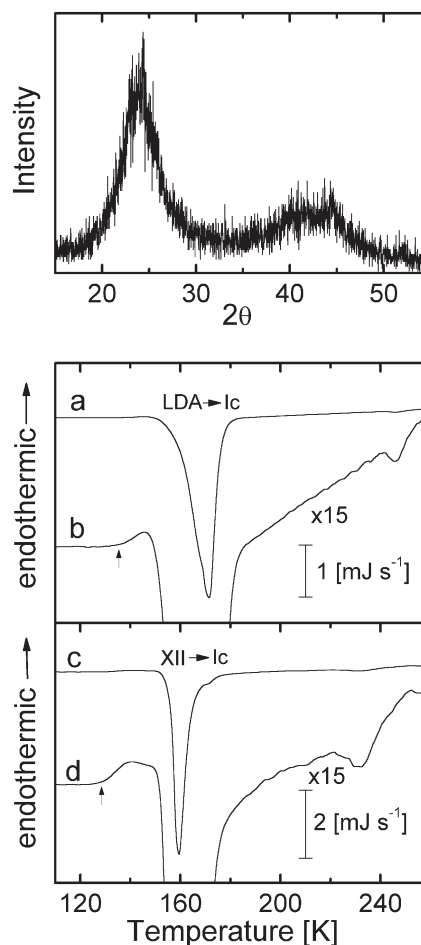


Fig. 7 Comparison of DSC features of LDA (a) with those of recovered ice XII made by compression of HDA at 77 K *via* pressure drop and shockwave heating (c). LDA was made from HDA on isobaric heating at 0.025 GPa up to 137 K, and its X-ray diffractogram shown on top (recorded at *ca.* 90 K, Cu-K α) agrees with that reported in the literature.^{6,7} Curve (a) is the DSC scan of LDA recorded, after annealing at 129 K for 90 min, on heating from 93 to 260 K, and (b) is curve (a) 15-fold enlarged. Curve (c) is the DSC scan of ice XII recorded, after annealing at 127 K for 180 min, on heating from 93 K to 260 K, and (d) is curve (c) 15-fold enlarged. The samples were cooled and heated at 30 K min⁻¹. The scans are normalized with respect to the samples' weights and shifted vertically for clarity. The ordinate bar is for (a) and 1 mg sample weight.

mol⁻¹ and 18 K for curve (c), and 127 K, 1.2 J K⁻¹ mol⁻¹ and 20 K for curve (d). After correction for thermal lag, T_{onset} is 131 K (c) and 125 K (d). From the DSC scans of 5 more samples recorded on first heating, T_{onset} is determined as 130 ± 1 K, ΔC_p as 1.7 ± 0.2 J K⁻¹ mol⁻¹, and width as 20 ± 1 K. We emphasize that these endothermic features were observed without prior annealing.

The effect of annealing on the thermal features of recovered ice V is shown in Fig. 9. The samples were heated and cooled at a rate of 30 K min⁻¹, and heating was started at 93 K. Annealing temperatures are marked by vertical bars, T_{onset} of endothermic features by arrows. Curve (a) is the scan of an ice V sample recorded, after annealing at 127 K for 90 min, on heating to 273 K. The endothermic step is superimposed by a weak endothermic peak. Curve (b) is the scan of a new sample recorded, after annealing at 127 K for 90 min, on first heating to 150 K, and curve (c) is the scan of the same sample recorded on second heating to 273 K. These two curves demonstrate the reversibility of the endothermic feature. Curve (d) is the scan of a new sample recorded, after annealing at 119 K for 90 min, on heating to 273 K and curve (e) the scan of another sample recorded, after annealing at

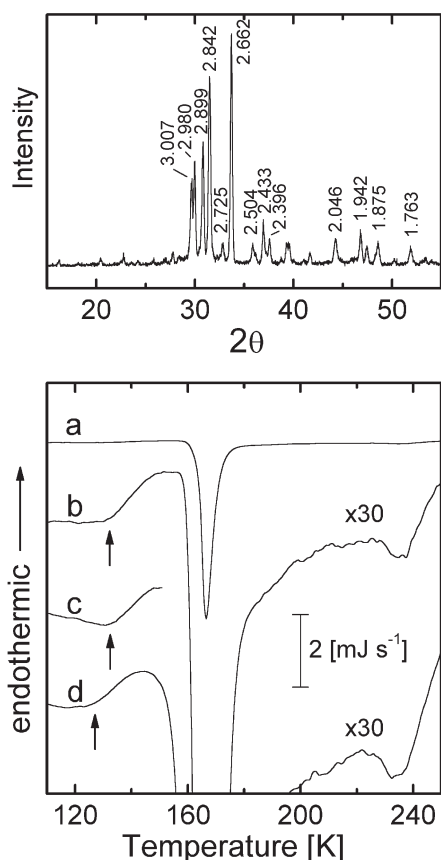


Fig. 8 DSC scans of recovered ice V made on compression of ice Ih to 0.64 GPa between 238–250 K, and subsequent cooling to 77 K at 0.64 GPa. Recovered ice V was characterized its X-ray diffractogram shown on top, and the d -spacings agree with those reported in ref. 35 (recorded at *ca.* 90 K, Cu-K α). (a) is the DSC scan recorded on heating from 93 K to 273 K, and (b) is (a) 30-fold enlarged. (c) is the scan of a new sample on first heating from 93 to 150 K, and (d) the scan of the same sample on second heating to 273 K, after cooling to 93 K ((c) and (d) 30-fold enlarged). The samples were cooled and heated at 30 K min⁻¹. The scans are normalized with respect to the samples' weights and they are shifted vertically for clarity. The ordinate bar is for (a) and 1 mg sample weight.

119 K for 180 min, on heating to 273 K. These two curves are nearly identical and thus, the doubling of annealing time has no effect.

Curve (f) is the scan of a new sample recorded, after annealing at 111 K for 90 min, on first heating to 150 K, and curve (g) is the scan of the same sample recorded on second heating to 273 K. Thus, the endothermic peak becomes most intense on annealing at 111 K (curve (f)), and it is absent on second heating without prior annealing (curve (g)). Curve (h) is the scan of a new sample recorded, after annealing at 103 K for 180 min, on first heating to 150 K, and curve (i) is the scan of the same sample recorded on second heating to 273 K. Annealing at 103 K shifts T_{onset} of the endothermic step to lower temperature, but it does not generate an additional endothermic peak as annealing at 111 K does (curve (f)). The maximal recovered enthalpy observed on annealing at 111 K is 30 J mol⁻¹ (curve (f)), and it is reduced to 12 J mol⁻¹ on annealing at 119 K (curves (d) and (e)).

Discussion

Once ice XII became available without contamination by HDA/LDA, the following thermal effects could be observed in the DSC scans *below* the ice XII \rightarrow ice Ic transition on heating the two types of recovered ice XII. For ice XII made

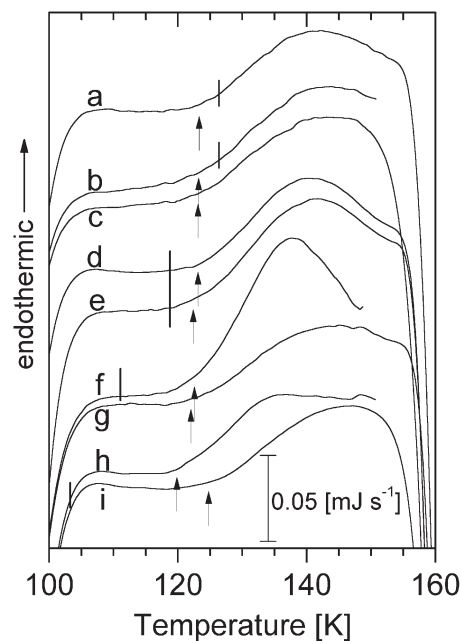


Fig. 9 Effect of T_{anneal} and t_{anneal} on the thermal features of recovered ice V (T_{anneal} is indicated by a vertical bar). Curve (a) is the scan recorded, after annealing at 127 K for 90 min, on heating from 93 to 273 K. Curve (b) is the scan of a new sample recorded, after annealing at 127 K for 90 min, on first heating from 93 to 150 K, and curve (c) is the scan of the same sample recorded on second heating. Curve (d) is the scan of a new sample recorded on heating, after annealing at 119 K for 90 min, and curve (e) is the scan of another sample recorded on heating, after annealing at 119 K for 180 min. Curve (f) is the scan of a new sample recorded, after annealing at 111 K for 90 min, on first heating from 93 to 150 K, and curve (g) is the scan of the same sample recorded on second heating. Curve (h) is the scan of a new sample recorded, after annealing at 103 K for 180 min, on first heating to 150 K, and curve (i) is the scan of the same sample recorded on second heating. The samples were cooled and heated at 30 K min⁻¹. The scans are normalized with respect to the samples' weights and shifted vertically for clarity. The ordinate bar is for a 1 mg sample weight.

by controlled isobaric heating of HDA, first, a reversible endothermic step resembling a glass \rightarrow liquid transition with T_{onset} of 130 K, ΔC_p of 1.9 J K⁻¹ mol⁻¹, and width of 10 K, and second, an endothermic peak after annealing between 103 and 119 K. For ice XII made on compression of ice Ih or HDA at 77 K *via* pressure drop and shockwave heating, these two effects are superimposed by a third thermal effect which is an irreversible exotherm with T_{min} at 133 (125) K on heating at 30 (10) K min⁻¹ (*cf.* Fig. 6). These three thermal effects are discussed as follows.

The irreversible exotherm with T_{min} at 133 (125) K

A basic difference between ice XII samples made on compression of ice Ih or of HDA at 77 K *via* pressure drops and shockwave heating, and those made by controlled isobaric heating of HDA up to *ca.* 183 K is that only in the former a pronounced exotherm is observable, with T_{min} at 133 \pm 2 (125 \pm 2) K for heating at 30 (10) K min⁻¹ (*cf.* Fig. 6, curves (a) and (b)). Whereas T_{min} is nearly constant in different samples, the evolved heat varies as 42 \pm 14 J mol⁻¹. The exotherm disappears on second heating and thus is an irreversible heat effect. Careful study by X-ray diffraction did not reveal any changes of the ice XII Bragg peaks on heating from 113 to 128 K (*cf.* Fig. 3 in ref. 16), and thus the exotherm is not caused by a phase transition. We surmise that this exotherm could be from stress/strain release in the recovered ice XII on heating. When HDA is pressurized at 77 K without indium linings, pressure drop can apparently generate a shockwave. This, in turn, leads to densification of the sample and transient local heating, up

into the metastability domain of ice XII.¹¹ The ice XII formed in this way is expected to contain stress/strain which is not, or only partially, released on cooling under pressure to 77 K. It is only released on heating at 1 bar and thus appears as an irreversible exotherm in the DSC scan.

Alternatively, differences between the rate of cooling and heating could be the cause. When a liquid is cooled at a higher rate through its glass transition region than it is heated subsequently for recording its DSC scan, an exothermic feature can develop below the onset temperature of a glass \rightarrow liquid transition (T_g) (cf. Fig. 1 in ref. 30). We extend the phenomenological similarity pointed out by Johari³⁶ between the behaviour of a glass on heating through its glass transition region, and the temperature dependence of proton order–disorder effects in ice and ice clathrates, to the effect of cooling *versus* heating rate. The weak exothermic feature observable on first heating in ice XII samples made by isobaric heating of HDA (cf. Fig. 2, curves (b) and (c)) is attributed to this effect, the cooling rate of *ca.* 50 K min⁻¹ being higher than the rate of heating at 30 K min⁻¹. In ice XII samples made on compression of ice Ih or HDA at 77 K *via* pressure drop and transient local heating into the metastability domain of ice XII (cf. Fig. 1 in ref. 11 and Fig. 3 in ref. 14), with the pressure vessel sitting in liquid N₂ during the whole procedure, the exotherm is much more intense and even hides the endothermic step (cf. Fig. 6). In this type of experiment the cooling rate cannot be measured but it is likely to be much higher than the rate of heating, and thus the exotherm could be more pronounced. We note that additional effects can occur when a sample is cooled under pressure and the DSC scan of the recovered sample recorded on subsequent heating at 1 bar which is the experimental setup used here. This is shown for polystyrene in Fig. 4.45 of ref. 37. Summarizing, we cannot unambiguously decide whether the pronounced exotherm with T_{\min} of 133 K shown in Fig. 6, curves (a) and (b), and the weak exothermic feature near T_{onset} in Fig. 2, curves (b) and (c), have the same origin.

General aspects of the endothermic features

Endothermic peaks in C_p *versus* T curves, or sigmoid-shape C_p -increase, recorded on heating were reported for ice Ih, ice Ic, ice V and ice clathrates, but these were only observed after prior annealing (reviewed in ref. 36). Thus, one of the most surprising aspects of this study is the observation of an endothermic step, or an increase in C_p with rising temperature, followed by a clear plateau region, in both ice XII and ice V samples recorded on heating *without* prior annealing (cf. Figs. 2 and 8) and it is to our knowledge the first example observed for a crystalline ice. Johari³⁶ recently analyzed “the origin of the heat capacity feature of annealed ices and ice clathrates”, and his paper should be consulted for details. He emphasizes the difference between sigmoid-shape C_p increase on heating an annealed sample of ice and ice clathrate, from that observed on glass softening or unfreezing of orientational disorder in a disordered crystal. Although the C_p features are remarkably similar, the underlying mechanism of the two differ. The first is attributable to complete disordering of those H₂O molecules which had become partially ordered during the course of annealing.³⁶ The maximum possible entropy for proton order-disorder transition is 3.37 J K⁻¹ mol⁻¹, which is also the residual entropy of fully proton-disordered ice Ih (*i.e.* Pauling entropy, ref. 38) and this value *does not* increase with temperature. “In contrast, the entropy of disorder, or the configurational entropy, of an orientationally disordered crystal without bonding restrictions, or that of a liquid with translational diffusion of molecules, is not easily determined by statistical methods, and its magnitude *does* increase with the temperature.” Thus, this variation of partially ordered and completely disordered H₂O molecules with temperature and time, and its freezing-in in a certain temperature range,

produces thermodynamic features qualitatively similar to those for glasses. Although the sigmoid-shape C_p increase on subsequent heating is determined by the rate of orientational diffusion of water molecules, its origin is distinguished from that observed for orientationally disordered crystals and glasses.³⁶ In this comparison the temperature marked here by arrows as T_{onset} for ice V or ice XII samples (cf. Figs. 2, 6, 7d and 8) where C_p begins to rise, is equivalent to T_g on heating a glass from its frozen-in nonequilibrium state into the supercooled (metastable equilibrium) liquid state.

Since for ice V detailed information is available on proton (deuteron) order–disorder and the effect of temperature,³⁹ we first discuss below our results obtained with recovered ice V samples. We then compare these with those obtained with recovered ice XII samples.

The endothermic step in the DSC scans of unannealed ice V

A recent neutron diffraction study of ice V under their thermodynamic conditions of stability had clearly indicated that partial ordering of the water molecule orientations already occurred at 254 K and 0.50 GPa, and that the degree of ordering increases gradually on cooling to 100 K (cf. Table III in ref. 39). An Arrhenius plot of these data in form of $\ln([\% \text{ order}]/[\% \text{ disorder}])$ *versus* $1/T$ gives a straight line which indicates that equilibrium had been (nearly) reached on the time scale of the experiment (not shown). Thus, when ice V is cooled at a certain rate, proton ordering increases with decreasing temperature,³⁹ by following a temperature dependent equilibrium between proton-ordering and disordering.

For our interpretation of the DSC features of unannealed ice V recorded on heating at 1 bar (cf. Fig. 8) it seems justified to assume also the existence of a temperature-dependent equilibrium between proton order and disorder, similar to that observed at 0.5 GPa,³⁹ albeit this equilibrium line at 1 bar may differ from that at 0.5 GPa with respect to % ordering at a given temperature and slope. On cooling ice V at a rate of 30 K min⁻¹ through a certain temperature region, the orientational diffusion time, which is needed for attaining an ordered arrangement of H₂O molecules, becomes much longer than the experiment's duration, and consequently a non-equilibrium state of proton order-disorder is frozen-in.³⁶ Upon reheating at the same rate, the structure responds sluggishly to the increase in temperature, and the enthalpy falls below the equilibrium value after crossing the equilibrium line.⁴⁰ Eventually, the orientational mobility becomes great enough to allow the relaxation rate to catch up with the heating rate, and the enthalpy rapidly converges on the equilibrium value (cf. Fig. 1 in ref. 40). This corresponds for ice V to a proton order \rightarrow disorder process. The ΔC_p increase with T_{onset} of 130 K (corrected) and width of 20 K indicates the temperature range where the orientational diffusion time becomes short enough for attaining thermodynamic equilibrium from the frozen-in nonequilibrium state. We note that T_{onset} is at 131 K on first heating (cf. (b) and (c) in Fig. 8), and it is lowered to 125 K on second and third heating (cf. (d) in Fig. 8). Annealing between 103 and 119 K has the same effect in shifting T_{onset} to *ca.* 125 K (cf. Fig. 9). This means that the orientational relaxation time had decreased at a given temperature. This is unlikely to be caused by the difference between the cooling rate of *ca.* -50 K min⁻¹ on quenching the ice V sample in the pressure vessel to 77 K, and the heating rate of 30 K min⁻¹ in the DSC instrument.⁴¹ This shift of T_{onset} to lower temperature on second heating, or after annealing, could be caused by diffusion of impurities into the ice V lattice, thus acting as extrinsic Bjerrum defects and lowering the Arrhenius energy. The effect of dissolved impurities such as CO₂ or N₂ gas onto the dielectric relaxation time and Arrhenius energy had been ascertained for ice Ih, and similar conclusions have been drawn for interpreting the dielectric relaxation time of ice V.⁴² These

extrinsic Bjerrum defects could be gaseous N₂ because, when the recovered ice V sample is filled under liquid N₂ into the DSC cell and the lid screwed on, considerable pressure buildup of gaseous N₂ could occur on heating and the N₂ penetrate the ice V lattice. Similar pressure buildup is unlikely in the high pressure vessel on cooling ice V to 77 K after its formation in the ice V domain.

The structural relaxation time calculated from a DSC scan obtained by heating at a rate of 30 K min⁻¹ is *ca.* 70 s at the onset temperature of the glass transition endotherm, and *ca.* 7 s at the midpoint temperature.⁴³ This gives us an estimate of the rate of orientational diffusion of water molecules (τ_{orient}) in ice V: thus, on first heating T_{onset} of 130 K corresponds to τ_{orient} of *ca.* 70 s, and T_{midpoint} of 140 K to *ca.* 7 s. On second heating T_{onset} shifts to 125 K (Fig. 8(d)), with corresponding τ_{orient} of *ca.* 70 s. This is consistent with Lobban and al.³⁹ inference that τ_{orient} at 125 K is less than 100 s (read from Fig. 6 in ref. 39). Recently Johari and Whalley⁴² reported from dielectric relaxation spectra of ice V that the dielectric relaxation time (τ_{diel}) is 1.5 s at 133 K. These two studies were carried out under pressure of 0.50 and 0.61 GPa.

On the assumption that the above relationship holds also here, we calculate an Arrhenius activation energy (E_a) for ice V of *ca.* 35 kJ mol⁻¹ for T_{onset} of 130 K and T_{midpoint} of 140 K (on first heating), and of *ca.* 32 kJ mol⁻¹ for T_{onset} and T_{midpoint} of 125 and 135 K (after annealing, *cf.* Fig. 9, curves (b) and (i)). Johari and Whalley⁴² reported from their study of the dielectric relaxation time of ice V under pressure of 0.61 GPa that E_a decreases from 49.9 kJ mol⁻¹ at 260 K, to 23.3 kJ mol⁻¹ at 160 K. They further argued that E_a may increase again at even lower temperatures (*cf.* their Fig. 4). It is possible that this has been observed here. For a detailed discussion of the mechanism of the temperature dependence of E_a in ice V ref. 42 should be consulted.

From the ΔC_p increase of the endothermic step and the width of the endotherm, the configurational entropy, ΔS_{conf} , could be calculated by integrating over the increase in heat capacity on a logarithmic temperature scale from T_{onset} to T_{endpoint} . We refrain from doing that because the error involved is too large.

The endothermic peak in the dsc scans of annealed ice V

Physical aging, or annealing, of a glass below its calorimetric glass \rightarrow liquid transition leads to relaxation of the structure toward a state of lower enthalpy and entropy, at a rate which decreases with decreasing temperature. This enthalpy relaxation becomes observable on reheating by DSC when the enthalpy recovery shows up as an endothermic peak.³⁰ For ice Ih, ice Ic, ice V and ice clathrates, the annealing effect and the spontaneous temperature rise on annealing a sample can also be considered in terms of enthalpy release toward the equilibrium line and a gradual proton ordering.³⁶ The appearance of a sigmoid shape endothermic C_p feature on heating an annealed sample can be considered in terms of enthalpy recovery when the orientational diffusion time becomes of the same order as the experimental time scale and the equilibrium state has been reached with respect to proton order–disorder.

The DSC scans of ice V samples annealed between 103 and 111 K show that the maximal heat effect is observed for T_{anneal} of 111 K (curve (f)). The endothermic heat effect of 30.3 J mol⁻¹ gives a ΔS_{conf} of 0.22 J K⁻¹ mol⁻¹ which corresponds to 6.5% of the Pauling entropy.

Our results are consistent with the more complete study by Handa, Klug and Whalley^{18,34} who had investigated in recovered ice V the effect of annealing by heat-flow calorimetry. Samples were annealed at ambient pressure at various temperatures in the range 103–120 K, and endothermic transitions observed on subsequent heating at 10 K h⁻¹ were attributed to

proton order–disorder transition. Handa *et al.*¹⁸ note that “the transition occurs in two regions, a principal peak in which most of the heat is absorbed, and a tail, possibly caused by a slower process, in which the rest of the heat is absorbed.” We have shown above that these two processes can be separated by comparing the DSC scans of unannealed ice V samples (*cf.* Fig. 8) with those of scans recorded after prior annealing (*cf.* Fig. 9).

The endothermic step in the DSC scans of unannealed ice XII

In the same manner we assume the existence of a temperature-dependent equilibrium between proton order and disorder for our interpretation of the DSC features of unannealed ice XII recorded on heating at 1 bar (*cf.* Fig. 2), and attribute the endothermic step observed in the DSC scans of unannealed ice XII to proton order–disorder transition as outlined above for ice V. T_{onset} of 130 K of the endothermic step indicates the temperature where on heating at 30 K min⁻¹ τ_{orient} of the water molecules becomes similar to the time scale of the experiment, and T_{end} of 140 K indicates the temperature where the equilibrium line had been attained. As pointed out above for ice V we do not know whether this equilibrium value corresponds to complete disorder, or to partial proton order.

T_{onset} and ΔC_p of the endothermic step are remarkably similar to those of ice V, but the width is only about half of it. τ_{orient} in ice XII is estimated as *ca.* 70 and *ca.* 7 s at T_{onset} and T_{midpoint} of 130 and 135 K (*cf.* above). For T_{onset} and T_{end} of 130 and 140 K, E_a is calculated as *ca.* 67 kJ mol⁻¹, which is twice the value for ice V.

The endothermic peak in the DSC scans of annealed ice XII

Annealing of ice XII samples has the same effect as shown for ice V, in that the enthalpy loss on annealing is recovered on reheating in form of an endothermic peak (*cf.* Figs. 3 and 4). This heat effect is maximal for T_{anneal} of 115 K (*cf.* Fig. 5a) which is close to T_{anneal} of 111 K observed for ice V (*cf.* Fig. 9 and ref. 18). The maximal value of recovered enthalpy of 0.21 J mol⁻¹ for annealing at 115 K for 120 min gives a ΔS_{conf} of 0.17 J K⁻¹ mol⁻¹ which corresponds to 5.0% of the Pauling entropy. On annealing above 115 K ΔH decreases for a given t_{anneal} (*cf.* Fig. 5a). This explains why annealing at 127 K does not give an endothermic peak on subsequent reheating (*cf.* Fig. 7b)

Proton ordering in ice V versus ice XII

A basic difference between ice V and ice XII is that the former can accommodate a large amount of proton order in its structure whereas ice XII cannot. The space symmetry of ice V ($A2/a$) allows partial ordering of the water molecule orientations, and Lobban *et al.*³⁹ reported ordering of up to 49% without reduction in symmetry (calculated from Table III). In contrast, the space symmetry of ice XII ($I\bar{4}2d$) constrains its structure to be fully proton-disordered. The latter case is reviewed by Kamb⁴⁴ where he points out that “space symmetry in combination with the ice rules for the H-bonds can constrain the proton site-occupancy to be exactly 1/2, implying long-range proton disorder in the Pauling sense.” Such a “constraint arises whenever an asymmetric H-bond contains a center of symmetry or passes through a twofold rotation axis or mirror plane, or whenever a water molecule is located at a site of $\bar{4}$ or 222 symmetry”. These criteria are met by the structure of ice XII. In ice XII O(1) lies on a $\bar{4}$ site symmetry,¹ which constrains the 4 adjacent H(3) hydrogen positions to be fully disordered (occupancy probability exactly $\frac{1}{2}$). Because of that, the remaining H(5) positions on O(1)–H(3)–H(5)–O(2) bonds have also to be fully disordered. Two H(4) positions on O(2)–H(4)–H(4)–O(2) have also to be fully disordered because of a twofold axis passing through the H-bond (p. 418 in ref. 45)

If our assignment of the endothermic features in the DSC scans of ice XII samples is correct, it follows that proton ordering can only be achieved by reduction of the space group symmetry to a new phase of ice. The proton ordering detected in recovered ice XII at low temperature by DSC appears to conflict with Raman spectra of similarly recovered ice XII where a single broad peak in the decoupled O–D (O–H) stretching band region had been attributed to proton disorder.¹² It appears that DSC is more sensitive than vibrational spectroscopy to detect modest amounts of proton order in an extensively disordered structure.

Neutron powder data of D₂O ice XII recorded at 260 K and 0.50 GPa were consistent with positional disordering of the hydrogen atoms.¹ The absence of modest amount of proton ordering could be due to the high temperature of 260 K. However, the second reported neutron diffraction study of D₂O ice XII was done at 1.5 K by Koza *et al.*,²⁴ and their analysis again revealed “a complete positional disorder in the proton sublattice of ice XII”. This seems to be contradictory to our interpretation of the DSC features of ice XII in terms of relaxation toward a temperature dependent proton order-disorder equilibrium. However, the sample of ice XII used for their study was made on compression of ice Ih at 77 K,²⁴ apparently *via* pressure drop and shockwave heating,¹⁰ and from the type of preparation it could well be a frozen-in state of proton disordered ice XII.

Comparison with proton ordering in ice Ih

Our observation of endothermic steps in unannealed ice V and ice XII samples attributable to proton order → disorder transition (*cf.* Figs. 2 and 8) raises the question why *unannealed* ice Ih does not show a similar endothermic step, and why annealing is required in order to observe a sigmoid shaped C_p increase on subsequent heating. Unannealed ice Ih would show such an endothermic step on heating at 30 K min⁻¹ if its T_{onset} , with τ_{orient} of *ca.* 100 s, is at a temperature where a proton order-disorder equilibrium exists which can be frozen-in on cooling and unfrozen on reheating. For “pure” ice Ih τ_{diel} of *ca.* 100 s is at *ca.* 150 K (read from Fig. 5.3 in *ref.* 2). But, in this temperature range ice Ih is completely disordered, and it requires lower temperatures to obtain partial ordering. This follows from the careful calorimetric study by Haida *et al.*⁴⁶ who measured heat capacities of “pure” ice Ih with an adiabatic calorimeter on annealing between 85 and 110 K, and observed C_p anomalies attributable to proton ordering. Their Fig. 2 shows that on heating to *ca.* 140 K these C_p anomalies had completely disappeared. Even between 90 and 140 K the C_p anomaly is only a minor effect, and S_{conf} corresponds in this temperature range to *ca.* 2 % of the Pauling entropy for complete proton ordering. Thus, at *ca.* 150 K there is no endothermic step because there is no proton order-disorder equilibrium line to depart from on cooling, and to attain on subsequent heating.

However, for ice Ih doped with KOH, the relaxation rate at low temperatures is enhanced enormously by the KOH and τ_{diel} of *ca.* 100 s is now at *ca.* 75 K (read from Fig. 5.10 in *ref.* 2). Thus, KOH doped ice Ih is sufficiently mobile for proton ordering and, after annealing several degrees below 72 K, C_p shows a peak at 72 K which marks the transition of ordered ice XI to disordered ice Ih.⁴⁷ This transition is not complete at 72 K, and a small excess C_p between 72 and *ca.* 100 K corresponds to *ca.* 5% of the Pauling entropy (see inset in Fig. 11.3 in *ref.* 2). Thus, an endothermic step might be observable for *unannealed* ice Ih doped with KOH on heating at 30 K min⁻¹, with T_{onset} of *ca.* 75 K. This experiment requires to start a DSC scan well below *ca.* 60 K which is not possible with our instrument. We note that ice Ih is comparable with ice XII in that its space symmetry constrains its structure to be fully proton-disordered.⁴⁴

It would be nice to pin down the difference between the temperature dependence of the proton order-disorder equilibrium in ice V and ice XII, to that in ice Ih to specific types of strained H₂O molecules in the ice V and ice XII structures. Lobban *et al.*³⁹ discuss for ice V the factors responsible for partial order in terms of hydrogen-bond strain and conclude that “it is highly unlikely that the observed partial order is purely related to O–O–O bond angle distortion”. They further argue that “it seems reasonable to assume that nonbonded interactions will also have an important influence on the ordering of the water molecules’ orientations”. Nonbonded interactions must be much more pronounced in the dense structures of ice V and ice XII than in the open ice Ih structure.

Comparison of ice XII with LDA

Koza *et al.*⁵ first reported in 1999 that on pressurizing ice Ih at 77 K not only HDA^{6,7} can be formed but also unexpectedly ice XII. They further pointed out that in the past contamination of HDA samples by crystalline impurities had been granted little attention, and that according to their experimental work these impurities correspond to ice XII (*cf.* *ref.* 8 in *ref.* 24). Only recently it became clear that ice XII can form on pressurizing ice Ih at 77 K *via* HDA, that this requires a pronounced pressure drop and shockwave heating, and that these can occur in the absence of indium linings.¹⁰ Thus, the endothermic step with T_{onset} of 129 K on heating at 30 K min⁻¹ attributed in our previous studies of pressure-amorphized ice Ih or ice Ic by DSC to LDA,^{19–23} has to be assigned instead to ice XII. This reassignment was possible only once we could characterize the recovered samples by X-ray diffraction. In Fig. 7 the comparison of the DSC features of LDA (curves a and b) with those of ice XII (curves c and d) shows that these can now be distinguished by the *ca.* 11 degree shift of T_{min} of the intense exotherm caused by the phase transition to ice Ic to higher temperature in going from ice XII (c) to LDA (a). In samples containing mixtures of ice XII and LDA, these exotherms appear as distinct peaks which allows to determine their relative amounts (*cf.* Figs. 1 and 2 in *ref.* 16). A further complication arises in DSC studies of ice XII made *via* pressure drop and shockwave heating and containing varying amounts of HDA that the exotherm with T_{min} of 133 (125) K from stress/strain release in ice XII can be mistaken for the exotherm from the HDA → LDA transition. Depending on how HDA is made, the HDA → LDA transition exotherm can occur between *ca.* 116–130 K on heating at a rate of *ca.* 2–4 K min⁻¹ (*cf.* Fig. 4 in *ref.* 9). Therefore, it is essential to study ice XII samples free of HDA, and in the following we take the absence of the LDA → ice Ic peak with a minimum at 166–167 K as indicator for that. When HDA is made on compression of ice Ih at 77 K and converted on heating to LDA, this minimum comes in our experience very reproducibly at 166 ± 2 K on heating at 10 K min⁻¹.¹⁶

Finally, we compare the DSC features of LDA shown in Fig. 7 and recorded on heating at 30 K min⁻¹, with those reported by Handa and Klug³³ for heating at 0.17 K min⁻¹. The ΔC_p increase of 0.7 J K⁻¹ mol⁻¹ calculated from Fig. 7, curve (b)), is the same as that of 0.7 J K⁻¹ mol⁻¹ in *ref.* 33. The increase in heat capacity starts at 135 ± 2 K for heating at 30 K min⁻¹ (b), and at 124 K for heating at 0.17 K min⁻¹ (*ref.* 33). We note that assignment of this endothermic step to a glass → liquid transition had recently been questioned and a higher T_g value of 165 ± 5 K had been proposed,⁴⁸ but this has also been refuted.⁴⁹

It is also clear now that our claim for “Two calorimetrically distinct states of liquid water below 150 K” (*ref.* 23) has lost its basis because the DSC features of one of the two states have to be reassigned to those of ice XII. The three amorphous forms of water of low density, namely LDA, hyperquenched glassy water (HGW) and vapor-deposited amorphous ice (ASW),

now have the same T_g value. A difference still exists in that for HGW and ASW ΔC_p is more than twice of that of LDA.^{50–52} Whether this difference persists on thermal cycling into the highly viscous liquid state, in the manner applied in, ref. 23 has to be determined in subsequent studies.

Acknowledgements

We are grateful to Prof. J. L. Finney for discussions and help in calculating % order in ice V, to Dr K. Wurst for help with crystallography, and to the “Forschungsförderungsfonds” of Austria for financial support (project No. 13930-PHY).

References

- 1 C. Lobban, J. L. Finney and W. F. Kuhs, *Nature (London)*, 1998, **391**, 268.
- 2 V. F. Petrenko and R. W. Whitworth, *Physics of Ice*, Oxford University Press, 1999.
- 3 M. O’Keefe, *Nature (London)*, 1998, **392**, 879.
- 4 I.-M. Chou, J. G. Blank, A. F. Goncharov, H.-K. Mao and R. J. Hemley, *Science (Washington, D. C.)*, 1998, **281**, 809.
- 5 M. Koza, H. Schober, A. Tölle, F. Fujara and T. Hansen, *Nature (London)*, 1999, **397**, 660.
- 6 O. Mishima, L. D. Calvert and E. Whalley, *Nature (London)*, 1984, **310**, 393.
- 7 O. Mishima, L. D. Calvert and E. Whalley, *Nature (London)*, 1985, **314**, 76.
- 8 O. Mishima, *J. Chem. Phys.*, 1994, **100**, 5910.
- 9 O. Mishima, *Nature (London)*, 1996, **384**, 546.
- 10 I. Kohl, E. Mayer and A. Hallbrucker, *Phys. Chem. Chem. Phys.*, 2001, **3**, 602.
- 11 T. Loerting, I. Kohl, C. Salzmänn, E. Mayer and A. Hallbrucker, *J. Chem. Phys.*, 2002, **116**, 3171.
- 12 C. Salzmänn, I. Kohl, T. Loerting, E. Mayer and A. Hallbrucker, *J. Phys. Chem. B*, 2002, **106**, 1.
- 13 C. G. Salzmänn, T. Loerting, I. Kohl, E. Mayer and A. Hallbrucker, *J. Phys. Chem. B*, 2002, **106**, 5587.
- 14 I. Kohl, C. G. Salzmänn, E. Mayer and A. Hallbrucker, in *New Kinds of Phase Transitions: Transformations in Disordered Substances*, 325–333, ed. V. V. Brazhkin, S. V. Buldyrev, V. N. Ryzhov and H. E. Stanley, NATO Science Series II. Mathematics, Physics and Chemistry, vol. 81, Kluwer Academic Publishers, Dordrecht, Netherlands, 2002.
- 15 C. G. Salzmänn, I. Kohl, T. Loerting, E. Mayer and A. Hallbrucker, *Can. J. Phys.*, 2003, **81**, 25.
- 16 I. Kohl, E. Mayer and A. Hallbrucker, *J. Phys. Chem. B*, 2000, **104**, 12102.
- 17 I. Kohl, PhD Thesis, University of Innsbruck, 2001.
- 18 Y. P. Handa, D. D. Klug and E. Whalley, *J. Phys. Colloq.*, 1987, **48**, 435.
- 19 A. Hallbrucker, E. Mayer and G. P. Johari, *J. Phys. Chem.*, 1989, **93**, 7751.
- 20 G. P. Johari, A. Hallbrucker and E. Mayer, *J. Phys. Chem.*, 1990, **94**, 1212.
- 21 E. Mayer, *J. Mol. Struct.*, 1991, **250**, 403.
- 22 G. P. Johari, A. Hallbrucker and E. Mayer, *J. Chem. Phys.*, 1991, **95**, 6849.
- 23 G. P. Johari, A. Hallbrucker and E. Mayer, *Science (Washington, D. C.)*, 1996, **273**, 90.
- 24 M. M. Koza, H. Schober, T. Hansen, A. Tölle and F. Fujara, *Phys. Rev. Lett.*, 2000, **84**, 4112.
- 25 A. Hallbrucker and E. Mayer, *J. Phys. Chem.*, 1987, **91**, 503.
- 26 A. Bizid, L. Bosio, A. Defrain and M. Oumezzine, *J. Chem. Phys.*, 1987, **87**, 2225.
- 27 M. A. Floriano, Y. P. Handa, D. D. Klug and E. Whalley, *J. Chem. Phys.*, 1989, **91**, 7187.
- 28 G. P. Johari, *Phys. Chem. Chem. Phys.*, 2000, **2**, 1567.
- 29 G. P. Johari, *J. Chem. Phys.*, 2000, **112**, 8573.
- 30 I. M. Hodge, *J. Non-Cryst. Solids*, 1994, **169**, 211.
- 31 I. M. Hodge and A. R. Berens, *Macromolecules*, 1982, **15**, 762.
- 32 Y. P. Handa, O. Mishima and E. Whalley, *J. Chem. Phys.*, 1986, **84**, 2766.
- 33 Y. P. Handa and D. D. Klug, *J. Phys. Chem.*, 1988, **92**, 3323.
- 34 Y. P. Handa, D. D. Klug and E. Whalley, *Can. J. Chem.*, 1988, **66**, 919.
- 35 J. E. Bertie, L. D. Calvert and E. Whalley, *J. Chem. Phys.*, 1963, **38**, 840.
- 36 G. P. Johari, *Chem. Phys.*, 2000, **258**, 277.
- 37 B. Wunderlich, *Thermal Analysis*, Academic Press, Boston, 1990.
- 38 L. Pauling, *J. Am. Chem. Soc.*, 1935, **57**, 2680.
- 39 C. Lobban, J. L. Finney and W. F. Kuhs, *J. Chem. Phys.*, 2000, **112**, 7169.
- 40 G. W. Scherer, *J. Non-Cryst. Solids*, 1990, **123**, 75.
- 41 C. T. Moynihan, A. J. Eastal and M. A. DeBolt, *J. Am. Ceram. Soc.*, 1976, **59**, 12.
- 42 G. P. Johari and E. Whalley, *J. Chem. Phys.*, 2001, **115**, 3274.
- 43 C. A. Angell and L. M. Torrell, *J. Chem. Phys.*, 1983, **78**, 937.
- 44 B. Kamb, in *Physics and Chemistry of Ice*, ed. E. Whalley, S. J. Jones and L. W. Gold, Royal Society of Canada, Ottawa, 1973, p. 25.
- 45 H. Arnold, in *Transformations in Crystallography*, ed. T. Hahn, Kluwer Academic Press, London, 1992.
- 46 O. Haida, T. Matsuo, H. Suga and S. Seki, *J. Chem. Thermodyn.*, 1974, **6**, 815.
- 47 Y. Tajima, T. Matsuo and H. Suga, *J. Phys. Chem. Solids*, 1984, **45**, 1135.
- 48 V. Velikov, S. Borick and C. A. Angell, *Science (Washington, D. C.)*, 2001, **294**, 2335.
- 49 G. P. Johari, *J. Chem. Phys.*, 2002, **116**, 8067.
- 50 G. P. Johari, A. Hallbrucker and E. Mayer, *Nature (London)*, 1987, **330**, 552.
- 51 A. Hallbrucker, E. Mayer and G. P. Johari, *Philos. Mag. B*, 1989, **60**, 179.
- 52 A. Hallbrucker, E. Mayer and G. P. Johari, *J. Phys. Chem.*, 1989, **93**, 4986.